Microstructure and Mechanical Behavior of Novel Rare Earth–Containing Pb-Free Solders

M.A. DUDEK,[1] R.S. SIDHU,[1] N. CHAWLA,[1,3] and M. RENAVIKAR[2]

1.—School of Materials, Fulton School of Engineering, Arizona State University, Tempe, AZ 85287-6006. 2.—Assembly Technology Development, Intel Corporation, Chandler, AZ 85226. 3.—E-mail: nikhilesh.chawla@asu.edu

Sn-rich solders have been shown to have superior mechanical properties when compared to the Pb-Sn system. Much work remains to be done in developing these materials for electronic packaging. In this paper, we report on the microstructure and mechanical properties of La-containing Sn-3.9Ag-0.7Cu alloys. The addition of small amounts of La (up to 0.5 wt.%) to Sn-Ag-Cu refined the microstructure by decreasing the length and spacing of the Sn dendrites and decreased the thickness of the Cu_6Sn_5 intermetallic layer at the Cu/solder interface. As a result of the change in the microstructure, Sn-Ag-Cu alloys with La additions exhibited a small decrease in ultimate shear strength but significantly higher elongations compared with Sn-Ag-Cu. The influence of $LaSn_3$ intermetallics on microstructural refinement and damage evolution in these novel solders is discussed. Our results have profound implications for improving the mechanical shock resistance of Pb-free solders.

Key words: Pb-free solder, rare-earth, ductility

INTRODUCTION

Global concern over the environmental impact and health effects of Pb-based solders in consumer electronics has led to the development of Pb-free solder alternatives. Sn-Ag-Cu alloy is one of the most promising Pb-free alloys for replacement of Pb-Sn solder.[1] It is superior to other Sn-rich alloys because of its relatively low melting temperature, superior mechanical properties, good solderability, and relatively low cost.[2] Although these materials are, in principle, suitable as replacements for Pb-Sn,[1] many issues still need to be addressed. These include a higher soldering temperature compared to Pb-Sn compositions, and, in particular, their lower ductility.[3,4] The lower ductility of the solder has important implications because it is directly related to mechanical shock and drop resistance.[5]

Rare earths (REs), such as Ce and La, have been used extensively for microstructural refinement and creep resistance in steel, cast iron, and aluminum alloys.[6–9] Preliminary studies on RE-containing solders, such as Sn-0.7Cu, Sn-Zn, Sn-Ag-Cu, Sn-3.5Ag, and Au-Sn, show a discrepancy in reported microstructures and mechanical properties.[10–18] For example, a study on Sn-Ag-Cu alloys with 0.1 and 0.25 wt.%Ce and La additions[12] reported RE-containing intermetallics in the microstructure, while another showed no evidence of discrete intermetallics being formed.[13] Furthermore, there is little evidence in the literature for the formation of homogeneous microstructures in these RE solders. The variability in microstructures can likely be attributed to a wide variety of processing parameters and procedures. In addition, the high affinity of RE elements with oxygen can also lead to oxidation of the RE precursors. Xia et al.,[14] for example, processed Sn-3.33Ag-4.83Bi with a nominal content of 0.5% RE mixture, by melting the precursor materials in air, in an Al_2O_3 crucible, protected by a eutectic salt. After processing, they found that the actual amount of RE in the solder was only 0.08 wt.%, indicating that most of the initial RE had oxidized.

In addition to the variability in processing and microstructures, a large discrepancy in mechanical properties is also present in the literature. Some studies report that RE additions increase the strength of Sn-Ag-Cu solders, with an accompanying decrease in strain to failure.[10,11,13,14,16–18] Other studies, however, have reported increases in strain to failure with small amounts of RE. Chen et al.,[12,15] for example, observed both an increase in tensile strength and elongation of Sn-Ag-Cu with RE additions up to 0.05 wt.% (a mixture of Ce and La). Upon increasing the concentration further, a decrease in the strain to failure was observed. The mechanisms for the observed behavior are not clear and have not been fully discussed.

Given the discrepancies in the literature, a thorough study quantifying the microstructure and mechanical properties of RE containing solder alloys is needed. In particular, special attention needs to be paid to the processing procedures

(Received March 10, 2006; accepted May 5, 2006)

employed and their relationship to microstructure. In this study, the effect of lanthanum additions (0.1 wt.% and 0.5 wt.%) on the microstructure and shear strength of a Sn-3.9Ag-0.7Cu alloy was investigated. Lanthanum was chosen due to its low melting temperature compared to other RE elements, its wide availability, and its relatively low cost. It will be shown that large strain to failures can be obtained with relatively small amounts of La addition (over 150% increase over conventional Sn-Ag-Cu). This improvement in ductility comes with a very small penalty in shear strength. The relationship between processing, microstructure, and mechanisms for deformation in these materials is discussed in detail.

MATERIALS AND EXPERIMENTAL PROCEDURE

Vacuum-melted ingots of Sn-Ag-Cu with varying amounts of La (0.1 wt.% and 0.5 wt.%) were prepared. A schematic illustrating the processing procedure is shown in Fig. 1. High-purity Sn-3.9Ag-0.7Cu ingots (Indium, Ithica, NY) were cut into small rectangular pieces (6.5 mm × 6.5 mm × 13 mm) and mixed with La shot, roughly 2–8 mm^3 in size (ESPI, Ashland, OR, 99.995% pure). Due to the reactive nature of pure La with oxygen, the materials were mixed in a quartz ampoule (12 mm in diameter) under a sealed glovebox with helium atmosphere. The quartz ampoule was then evacuated to 10^{-5} Torr and sealed. The sealed ampoules were heat treated at 1,000°C for 4 h, and periodically mixed by rotation of the ampoule, in order to homogenize the liquid metal. The ampoules were then water quenched, removed from the ampoule, and sectioned.

Microstructure characterization was conducted on the as-processed ingot material, as well as after reflow of the solder joints. Ingots were sectioned and polished to a final finish of 0.05 μm colloidal silica. Optical microscopy, scanning electron microscopy (SEM), transmission electron microscopy (TEM), and image analysis were conducted to quantify the microstructure. These included secondary Sn dendrite size and arm spacing and $LaSn_3$ intermetallic size and spacing. Energy dispersive spectroscopy (EDS) analysis was also used to confirm the composition of the La-containing intermetallic. The TEM sample preparation was conducted by polishing samples to a thickness of about 100 μm, dimpling, and ion milling. Ion milling was conducted using a liquid nitrogen-cooled stage to minimize sample heating.

Quantitative microstructure characterization was conducted using image analysis software (ImageJ, Gaithersburg, MD). Both optical and SEM micrographs were segmented into black and white images. The intermetallic phases of interest were fit to ellipses to estimate their size and aspect ratio. Interparticle spacing was calculated using a finite-body tessellation method. In this method, a near-neighbor distance is defined as the shortest distance between two particles that share a cell wall

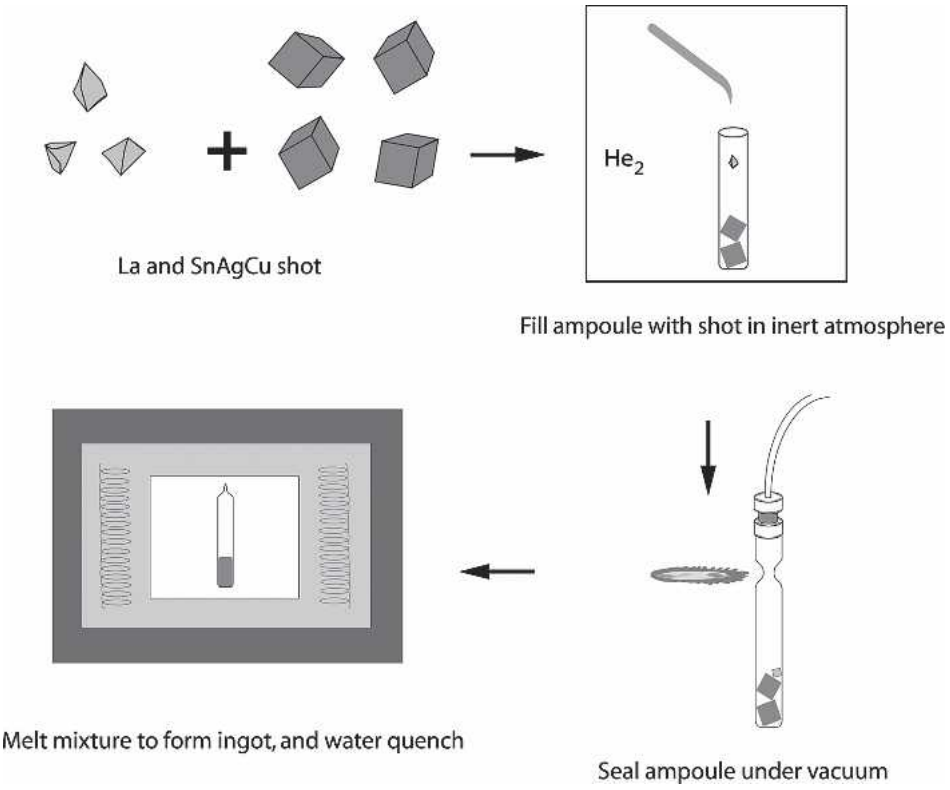

Fig. 1. Schematic illustration of the processing procedure for the La-containing Sn-Ag-Cu Pb-free solder.

in the tessellated image.[19–23] It is also of importance to quantify the distribution in nearest neighbor spacing within the microstructure, in order to determine the degree of particle clustering. The degree of clustering can be determined using a coefficient of variance technique (COV_d):

$$COV_d = \frac{\sigma_d}{d} \quad (1)$$

where σ_d^2 is the variance in the mean nearest-neighbor distance, and d is the average of the mean near-neighbor distance.[24]

Differential scanning calorimetry (DSC) was used to determine the melting point of the solder with La addition. The measurements were conducted in a dry argon atmosphere gas. The calorimeter (Perkin Elmer DSC-7, Boston, MA) was calibrated prior to testing using a standard high-purity indium sample. Samples of 20–40 mg were prepared from the as-cast material and were ultrasonically cleaned in acetone. Samples were weighed and placed into Al_2O_3 crucible pans. An empty Al_2O_3 crucible was used as a reference. Samples were then heated and cooled at a rate of 1°C/min. in the temperature range of 25–600°C.

Mechanical testing was conducted on solder/Cu single lap shear joints. As-processed solder ingots were machined into 6.35 mm × 6.35 mm × 0.5 mm squares. These were lightly polished to remove oxidation caused by the machining process, and ultrasonically cleaned in acetone. Oxygen free copper bars (50.8 mm and 6.35 mm in thickness) were polished to a 0.05 μm finish with colloidal silica solution, and etched in 2 vol.% nitric acid for 10 sec to remove residual oxides. A graphite mask was applied to the Cu bars, leaving a 6.35 mm × 6.35 mm area for reflow. A rosin mildly activated (RMA) flux was applied to the unmasked portions of the Cu bars to improve wetting between the Cu and the solder. The joint was assembled with the aid of a reflow fixture, to minimize misalignment and maintain a consistent joint solder thickness of approximately 500 μm.[25] The entire assembly was heated on a hot plate and held at 120°C for 20 min. to allow excess flux to vaporize. The temperature was then raised until the solder reached 220°C and was held for 40 sec (temperature not exceeding 240°C). The assembly was then removed from the hot plate and air cooled on an aluminum heat sink. The temperature in the solder was monitored using a thermocouple, and a reproducible cooling rate of 0.7°C/s was obtained. The cooling rate was measured from the peak temperature to 150°C, because the joint microstructure does not change significantly below this temperature during cooling.[26–28] Shear testing was conducted using a servo-hydraulic load frame at room temperature and a shear strain rate of 10^{-3} s^{-1}. The strain was measured using an extensometer with a gage length of 10 mm. Fractographic analysis of the shear strength testing specimens was conducted by SEM.

RESULTS AND DISCUSSION

Differential Scanning Calorimetry

The DSC was employed to determine the effect of small amounts of La on the melting characteristics of Sn-Ag-Cu. Figure 2 shows the heat flow versus temperature melting curves, on heating, for Sn-3.9Ag-0.7Cu and Sn-3.9Ag-0.7Cu-0.5La. Both curves show a single melting peak (endothermic), with the onset temperature around 217°C, indicating that La had little effect on the reflow temperature of the eutectic solder. In the Sn-3.9Ag-0.7Cu-0.5La alloy, however, small peaks can be seen between 325°C and 350°C. Judging by the Sn-La phase diagram, this appears to be a reasonable temperature range for melting of the small amount of $LaSn_3$ (~2.5 vol.%). The endothermic peak in the Sn-3.9Ag-0.7Cu-0.5La curve at ~335°C indicates that $LaSn_3$ is the primary intermetallic in this alloy, and that at standard reflow temperatures, $LaSn_3$ will remain present in the melt.

Microstructure Characterization

As-processed Microstructure

Representative microstructures of as-processed Sn-3.9Ag-0.7Cu, Sn-3.9Ag-0.7Cu-0.1La, and Sn-3.9Ag-0.7Cu-0.5La are shown in Fig. 3. As expected, the microstructure of near-eutectic Sn-Ag-Cu alloy consisted of Sn-dendrites and a eutectic mixture of Ag_3Sn and Cu_6Sn_5 intermetallics distributed in the Sn-rich matrix.[29–32] The microstructure of the La-containing solders consisted of discrete, homogeneously distributed $LaSn_3$ (Fig. 3b and c). The Sn-La phase diagram predicts the formation of an intermetallic phase, $LaSn_3$, for Sn concentrations greater than 72wt.%Sn.[33] The EDS analysis of the particles yielded an atomic ratio between Sn and La of approximately 3:1, confirming the composition of the particles as $LaSn_3$.

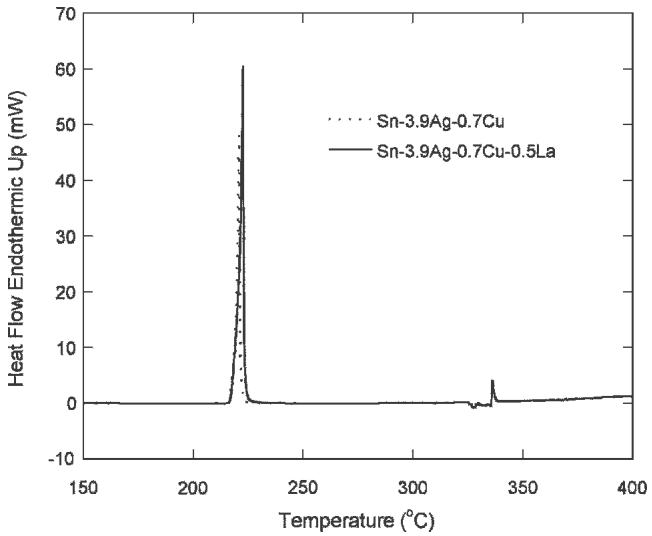

Fig. 2. Heat flow versus temperature curve for Sn-3.9Ag-0.7Cu and Sn-3.9Ag-0.7Cu-0.5La, heating cycle.

Figure 4 shows a comparison of higher magnification SEM micrographs. Figure 4b shows the microstructure of a furnace-cooled Sn-3.9Ag-0.7Cu-0.5La alloy, in which the $LaSn_3$ intermetallics are approximately 75 μm in size. In conventional Sn-Ag-Cu alloy, Ag_3Sn and Cu_6Sn_5 intermetallic phases were observed. In the La-containing solder, the $LaSn_3$ intermetallics had a characteristic faceted geometry, also referred to as "Chinese scripts," which have also been observed in other systems.[34–37] Recent analysis by Dudek and Chawla[38] on furnace-cooled alloys, using three-dimensional visualization techniques, showed that the $LaSn_3$ intermetallics are actually complex dendrites. The formation of the faceted geometry can be attributed to a combination of factors including solid/liquid interface stability during diffusional growth, the orientation dependence of interface energy (i.e., certain growth planes will dominate to minimize total surface energy, and from differences in growth rates due to atomic arrangement in the planes), and the minimization of strain energy due to volume changes associated with differences in structure and bonding between solid and liquid phases.[39]

The $LaSn_3$ phases are considerably larger in size than the other intermetallic phases, are present in the eutectic, and surround the boundaries of the Sn dendrites. Figure 3 clearly shows that there is some microstructural refinement of the Sn matrix in the La-containing alloys, compared with the base Sn-Ag-Cu alloy. This is exemplified by the quantitative measurements shown in Table I, which include size, spacing, aspect ratio, and degree of clustering of $LaSn_3$ for both 0.1 and 0.5wt.%La. As discussed previously, the degree of clustering in the microstructure can be determined using a coefficient of variance technique (COV_d), in which the variance in the nearest neighbor spacing is divided by the mean nearest neighbor spacing. The Sn dendrite length and spacing for all alloys is also shown. At 0.5wt.%La, for example, the Sn dendrite length is approximately 60% smaller than for 0 wt.%. A comparison of Sn-3.9Ag-0.7Cu-0.1La and Sn-3.9Ag-0.7Cu-0.5La shows that the size and distribution of $LaSn_3$ intermetallics differ. Sn-3.9Ag-0.7Cu-0.1La alloy has smaller $LaSn_3$ particles. which are more homogeneously distributed from the COV analysis.

Yu et al.[13] also showed a marked refinement in Sn dendrite length and spacing with a 0.25% RE (mixture of Ce and La). They did not, however, show the presence of any RE-rich phases, stating that this small amount remains in solution in Sn. This

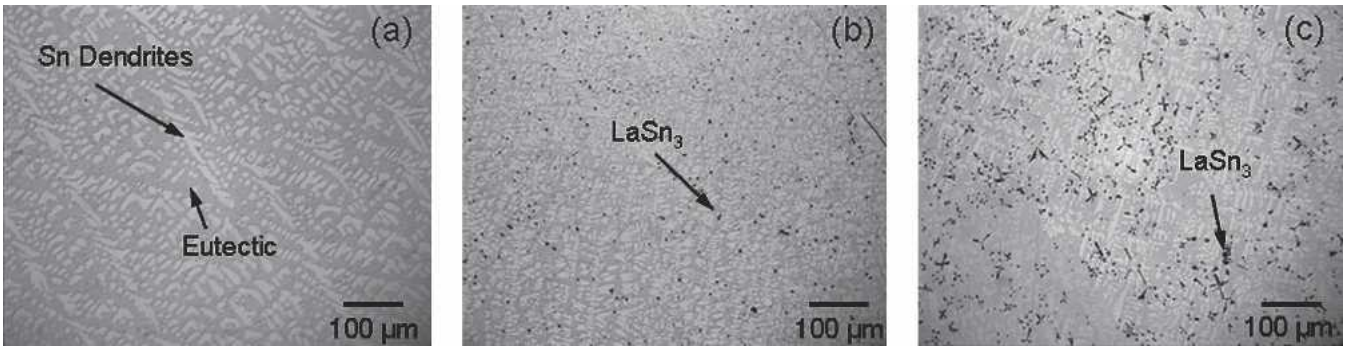

Fig. 3. Optical micrographs of as-processed ingots of (a) Sn-3.9Ag-0.7Cu, (b) Sn-3.9Ag-0.7Cu-0.1La, and (c) Sn-3.9Ag-0.7Cu-0.5La showing the homogeneous distribution of $LaSn_3$ intermetallics and the refinement in Sn dendrite size and spacing, with La addition.

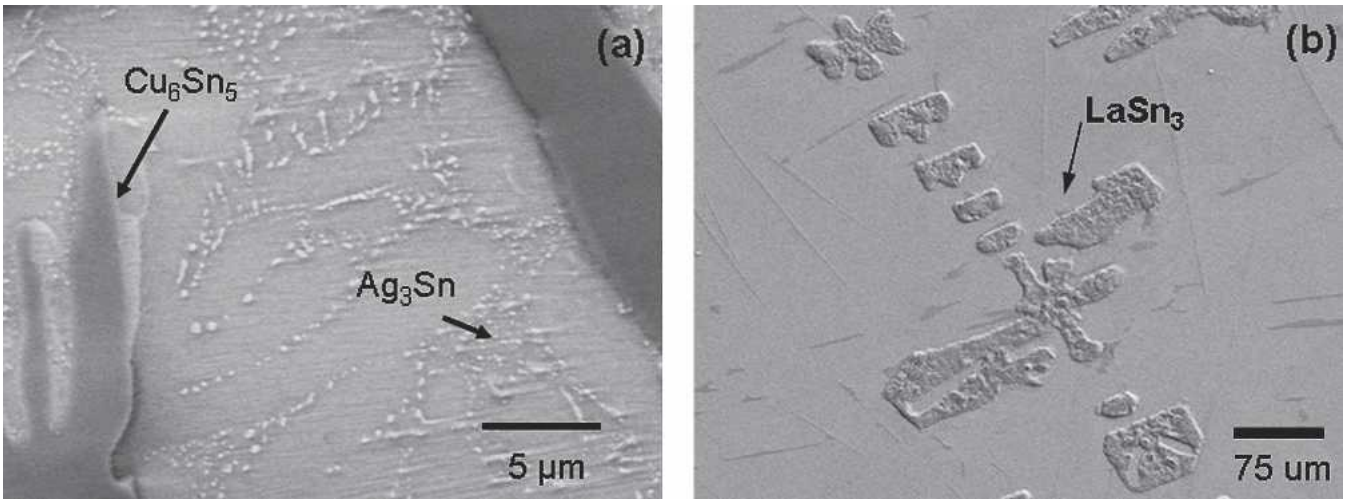

Fig. 4. (a) Backscattered SEM micrographs of Sn-3.9Ag-0.7Cu alloy highlighting Cu_6Sn_5 and pure Sn dendrites decorated by a eutectic region of Ag_3Sn in a Sn matrix. (b) Micrograph of Sn-3.9Ag-0.7Cu-0.5La alloy highlighting the $LaSn_3$ intermetallics, which exhibit a dendritic structure.

finding does not seem to agree with the phase diagrams for both Ce-Sn and La-Sn, which show practically no solubility between the two elements.[33] Furthermore, Huang et al.[40] determined the solubility of La in Sn at 232°C to be about 0.046 wt.%.

Let us now address the evolution of microstructure during solidification. In the base Sn-Ag-Cu alloy, at the reflow temperature of ~240°C, Sn is melted and the Sn-Ag-Cu eutectic phases dissolve. Upon cooling, solidification begins with nucleation and growth of Sn dendrites. Complete solidification occurs with the formation of the eutectic mixture (Ag_3Sn and Cu_6Sn_5 in a Sn matrix). The driving force for Sn dendrite solidification is the large undercooling present in these alloys.[29] With small additions of La, growth of Sn grains appears to take place by heterogeneous nucleation at $LaSn_3$ particles. This is supported by transmission electron microscopy of the as-processed Sn-3.9Ag-0.7Cu-0.5La material, shown in Fig. 5. $LaSn_3$ (larger dark particle) is characterized by an $L1_2$ crystal structure, as shown by the diffraction pattern. The Sn grains can be seen adjacent to the facets of the $LaSn_3$ particle, and their size and orientation correlate well with the length of the faceted edges of the $LaSn_3$ particles. We can deduce that the Sn grains are in fact nucleating and growing from the faceted edges of the $LaSn_3$ intermetallics. The large amount of heterogeneous nucleation sites provided by the $LaSn_3$ would appear to explain the decrease in size of Sn dendrites in the La-containing solders, observed in Fig. 3.

Reflowed Microstructure

The previous section described the microstructure of the solders, with and without La addition, in the as-processed condition. In this section, we describe the microstructure of solders after reflow. The as-reflowed microstructures of the solder joints are shown in Fig. 6. The microstructure of the joints

Table I. Summary of Microstructural Characterization Results for As-Processed Solder Alloys

	Concentration of La (Wt.%)		
	0	**0.1**	**0.5**
$LaSn_3$ characteristics			
Volume fraction (%)	N/A	0.8 ± 0.1	2.4 ± 0.2
Major axis (μm)	N/A	2.7 ± 0.1	3.7 ± 2.5
Minor axis (μm)	N/A	1.90 ± 0.08	1.7 ± 0.7
Aspect ratio	N/A	1.40 ± 0.03	2.10 ± 0.02
Interparticle spacing (μm)	N/A	23.5 ± 1.4	10.9 ± 0.9
Degree of clustering (coefficient of variance of interparticle spacing)	N/A	0.40 ± 0.05	0.60 ± 0.03
Sn-rich matrix characteristics			
Dendrite length (μm)	27.7 ± 10.2	11.3 ± .2	12.9 ± 3.1
Dendrite spacing (μm)	17.1 ± 5.5	6.7 ± 1.9	7.5 ± 2.4

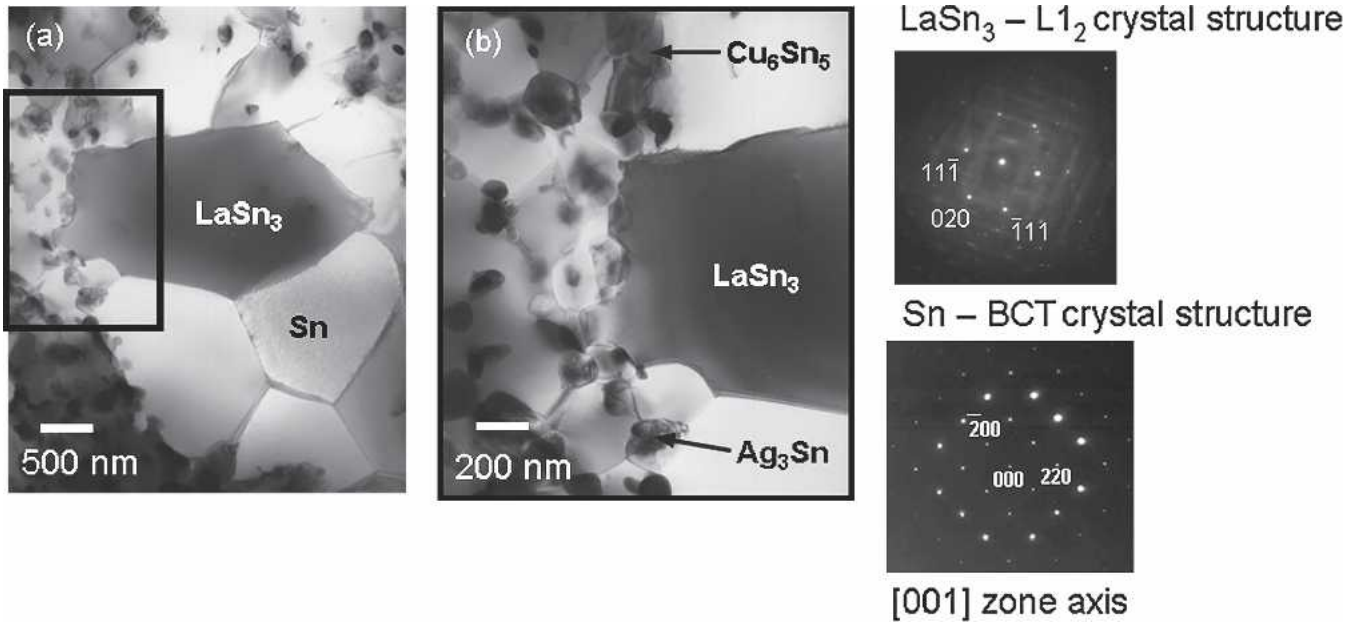

Fig. 5. TEM micrographs and diffraction patterns from as-processed Sn-3.9Ag-0.7Cu-0.5La (a) showing the eutectic microstructure consisting of Ag_3Sn and Cu_6Sn_5 intermetallics surrounded by a Sn matrix and dendritic Sn grains nucleating from the faceted edges of the $LaSn_3$ intermetallic. (b) Higher magnification of inset from (a).

are coarser than that of the as-processed material due to the somewhat slower cooling rate, allowing more time for Sn-dendrite and intermetallic growth. The Ag_3Sn particles exhibited a spherical morphology, similar in size to that in the as-processed material. Relatively large Cu_6Sn_5 particles (~25 μm) were also observed in the eutectic region. Table II shows quantitative measurements of $LaSn_3$ and Ag_3Sn size and aspect ratio. It also shows measurements of Sn dendrite size and dendrite arm spacing. A comparison to Table I, which contains measurements in the as-processed condition, shows that the $LaSn_3$ intermetallics do not undergo significant coarsening or segregation during the reflow process (relative to the as-processed condition). This is expected, because the reflow temperature is not high enough to melt the $LaSn_3$ intermetallics. Note that the La-containing solders still have a finer Sn dendrite structure, after reflow, when compared with the Sn-Ag-Cu base material.

The interface between the solder and Cu substrate for all alloys is characterized by the formation of a thin Cu_6Sn_5 intermetallic layer upon reflow[25,41] (Fig. 7). This intermetallic layer is characterized by a nodular or planar morphology.[19,25,28] It is interesting to note that in the La-containing alloys, the intermetallic thickness has decreased by approximately 60% compared with the Sn-Ag-Cu alloy. This result could have a substantial impact on the mechanical behavior of the joints, because the thickness of this intermetallic layer affects the properties of solder/Cu joints.[42] We believe that the reason for lower intermetallic thickness of Cu_6Sn_5 is as follows. Given that $LaSn_3$ contributes to heterogeneous nucleation of Sn, the Sn dendrites solidify more quickly. Thus, the solder remains in liquid state for a lower time, which equates to less time for reaction with the Cu substrate, and a lower intermetallic thickness.

Shear Behavior

In this section, we discuss the shear properties of the solder alloys. The shear behavior of Sn-3.9Ag-0.7Cu, Sn-3.9Ag-0.7Cu-0.1La, and Sn-3.9Ag-0.7Cu-0.5La is shown in Fig. 8.

Table III summarizes the shear behavior of the joints. The ultimate shear strength decreased slightly with increasing La concentration. The La-containing alloys are quite damage tolerant in nature, however, the decreases in stress after the ultimate shear strength are quite gradual and not abrupt (as is the case for Sn-Ag-Cu). The slow decrease in stress with increasing strain in the curves makes determining the strain to failure difficult. In order to quantitatively compare the strains at failure, a procedure was developed to determine the onset of failure. The strain to failure was taken as a deviation of 5% from a linear regression fit to the end of the stress-strain curve. More importantly, the strain

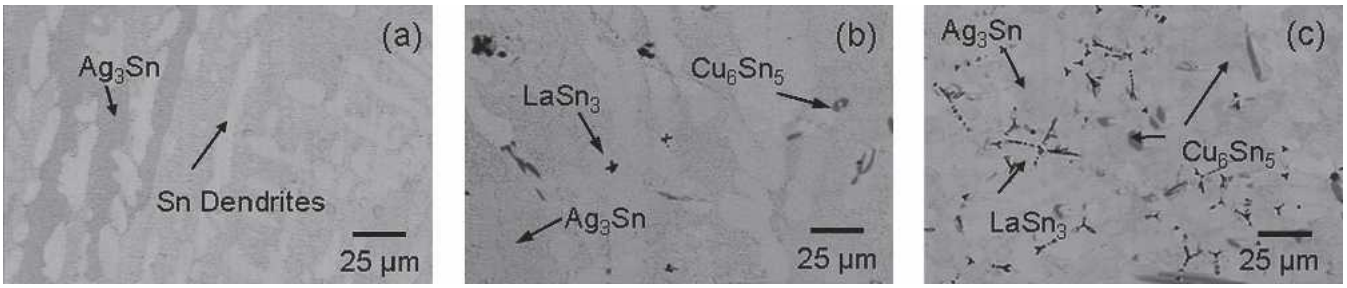

Fig. 6. SEM micrographs of reflowed joints for (a) Sn-3.9Ag-0.7Cu, (b) Sn-3.9Ag-0.7Cu-0.1La, and (c) Sn-3.9Ag-0.7Cu-0.5La.

Table II. Summary of Microstructure Characterization for Reflowed Solder Joint Systems

	Concentration of La (Wt.%)		
	0	**0.1**	**0.5**
$LaSn_3$ characteristics			
Major axis (μm)	N/A	2.9 ± 0.3	3.9 ± 2.1
Minor axis (μm)	N/A	1.7 ± 0.1	1.4 ± 0.9
Aspect ratio	N/A	1.7 ± 0.1	2.7 ± 0.1
Interparticle spacing (μm)	N/A	20.3 ± 1.5	10.9 ± 0.9
Degree of clustering (coefficient of variance of interparticle spacing)	N/A	0.41 ± 0.06	0.62 ± 0.04
Sn-rich matrix characteristics			
Sn secondary dendrite length (μm)	41.8 ± 39.5	14.0 ± 4.9	20.5 ± 12.1
Sn secondary dendrite spacing (μm)	12.6 ± 5.3	11.2 ± 3.1	9.0 ± 3.2
Joint characteristics			
Cu_6Sn_5 intermetallic thickness (μm)	5.5 ± 1.6	2.1 ± 0.4	2.7 ± 0.8

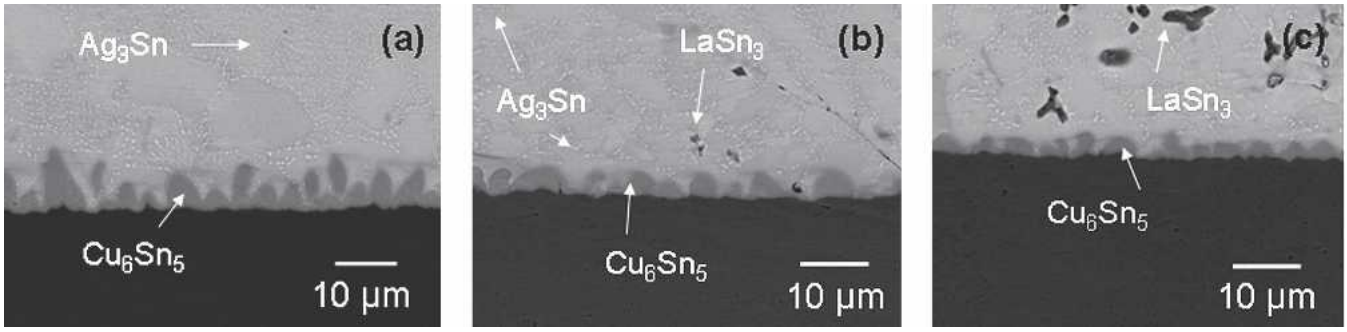

Fig. 7. Representative SEM micrographs of the Cu substrate/solder interface in reflowed joints for (a) Sn-3.9Ag-0.7Cu, (b) Sn-3.9Ag-0.7Cu-0.1La, and (c) Sn-3.9Ag-0.7Cu-0.5La.

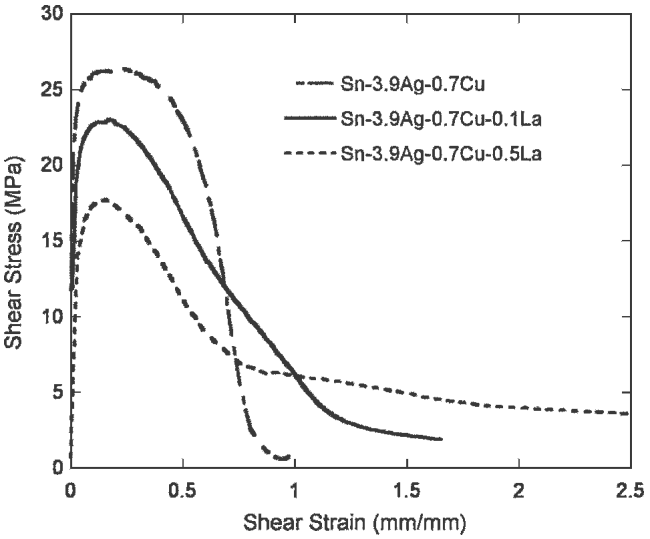

Fig. 8. Shear stress versus shear strain curves for Sn-3.9Ag-0.7Cu, Sn-3.9Ag-0.7Cu-0.1La, and Sn-3.9Ag-0.7Cu-0.5La tested in monotonic shear.

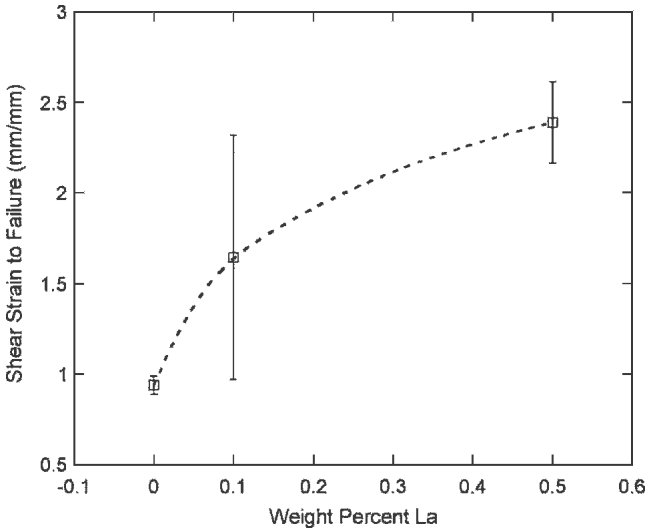

Fig. 9. Strain to failure versus wt.% La, showing an asymptotic relationship, indicating the presence of a critical La concentration for improving ductility.

Table III. Monotonic Shear Results for Sn-3.9Ag-0.7Cu, Sn-3.9Ag-0.7Cu-0.1La, and Sn-3.9Ag-0.7Cu-0.5La

Alloy	Ultimate Shear Strength (MPa)	Strain to Failure (%)
Sn-3.9Ag-0.7Cu	26.8 ± 0.2	94 ± 5
Sn-3.9Ag-0.7Cu-0.1La	23.4 ± 1.4	164 ± 67
Sn-3.9Ag-0.7Cu-0.5La	17.3 ± 0.5	239 ± 22

to failure of Sn-3.9Ag-0.7Cu-0.5La samples increased significantly, nearly 150%, over that of Sn-3.9Ag-0.7Cu. Chen et al.[12] also observed an increase in the elongation of Sn-Ag-Cu tensile samples with RE addition (mainly Ce and La) up to 0.1 wt.%; however, no explanation was offered for the observed behavior.

The effect of increasing plasticity with increasing La content is not linear in nature, and rather exhibits an asymptotic behavior, as shown in Fig. 9. This indicates the presence of a critical concentration for La, beyond which there will likely not be an appreciable improvement in ductility.

Examination of the fractured surfaces of the joints (Fig. 10) revealed a classical void nucleation, growth, and coalescence process in the Sn-3.9Ag-0.7Cu-0.5La, where the bottom of most dimples contained $LaSn_3$ intermetallics. Note that fracture occurred through the solder, away from the Cu_6Sn_5 intermetallic/solder interface. The resulting fracture path was relatively tortuous in nature, with visible steps on the fracture surface. Sn-3.9Ag-0.7Cu exhibited more of a tearing type of fracture morphology with feature sizes (voids developed during fracture) that were much smaller than that in Sn-3.9Ag-0.7Cu-0.5La. Fracture in Sn-3.9Ag-0.7Cu occurred at the interfacial region between the solder and the Cu_6Sn_5 intermetallic, exposing the tips of the Cu_6Sn_5 nodules in some areas.[25] Sn-3.9Ag-0.7Cu-0.1La appears to behave more similarly to Sn-3.9Ag-0.7Cu, with fracture also occurring along the interfacial region. Voids caused by the fracture process are also much smaller in scale than for the Sn-3.9Ag-0.7C-0.5La joints, although there is evidence for the presence of $LaSn_3$ at the base of the voids.

We believe that the increase in ductility with increasing La concentration is caused by the ability

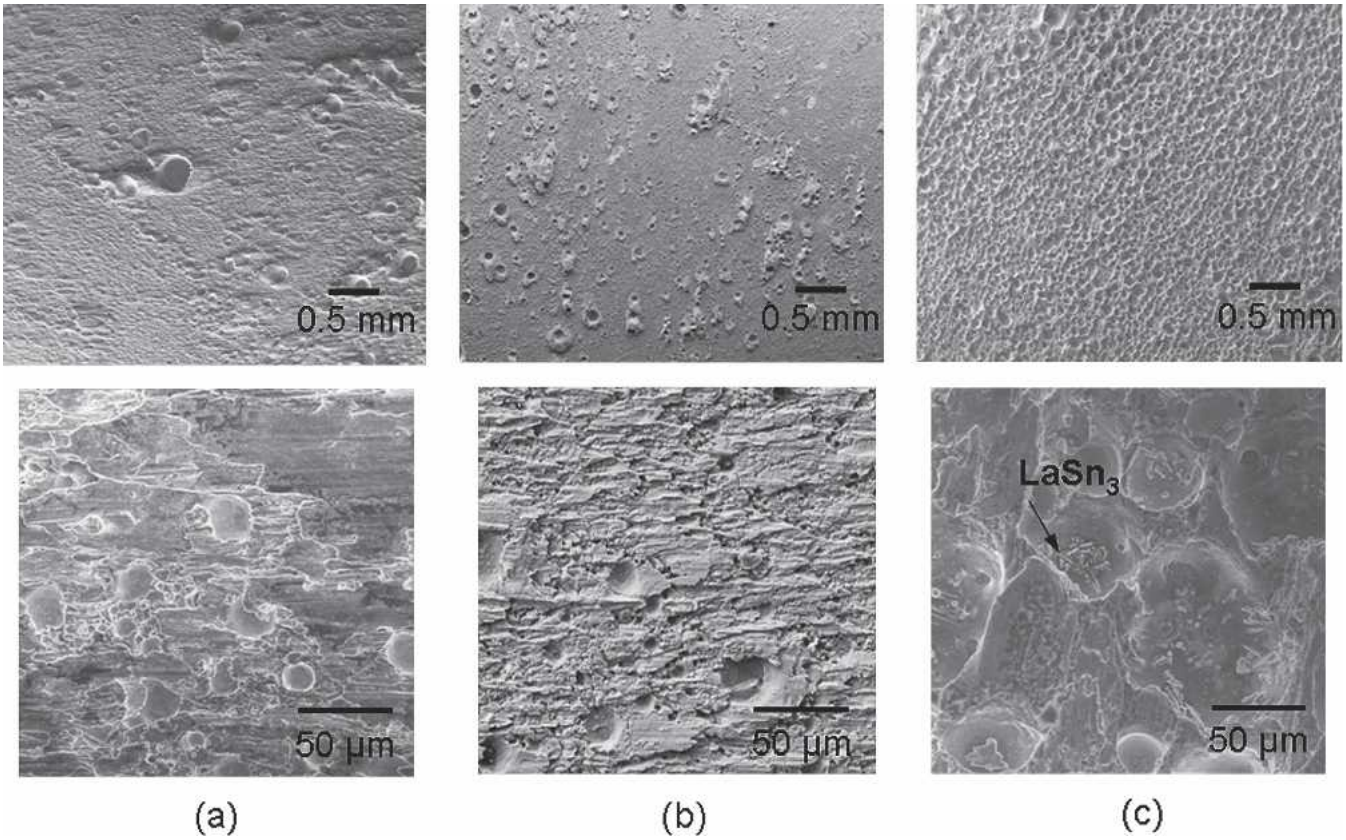

Fig. 10. Fracture surfaces of lap shear samples for (a) Sn-3.9Ag-0.7Cu, (b) Sn-3.9Ag-0.7Cu-0.1La, and (c) Sn-3.9Ag-0.7Cu-0.5La.

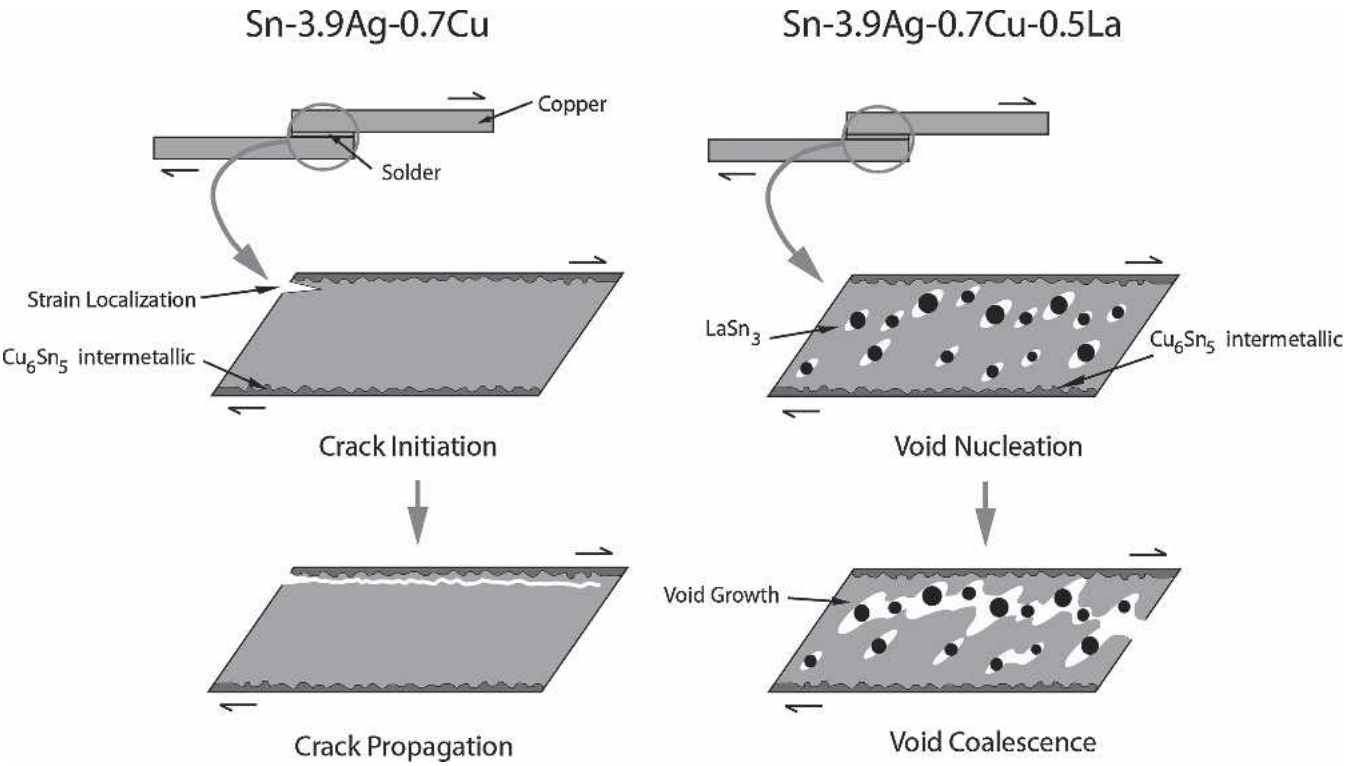

Fig. 11. Damage accumulation schematic for Sn-3.9Ag-0.7Cu and Sn-3.9Ag-0.7Cu-0.5La showing the ability of the $LaSn_3$ intermetallic to nucleate and grow voids during fracture, resulting in a more torturous crack path and minimizing crack propagation along the brittle Cu_6Sn_5 intermetallic/solder interface.

of the $LaSn_3$ intermetallics to nucleate and grow voids in the solder interior, dominating the fracture process and minimizing crack growth along the brittle Cu_6Sn_5 intermetallic/solder interface. Figure 11 is a schematic of the likely fracture mode for the La-containing solders. Crack propagation along the intermetallic interface in the 0.5 wt.%La-containing samples does not take place. This is likely a result of stresses within the solder being more homogeneously distributed and not concentrated at the intermetallic/solder interface. Thus, in Sn-Ag-Cu, fracture is localized to a very small fraction of the joint. The addition of La, however, allows deformation to be "spread out" over the entire joint volume, which results in a higher macroscopic ductility.

Such enhanced ductility has profound implications for improving the mechanical shock resistance (such as drop failure) of electronic packages containing Sn-Ag-Cu solders.

CONCLUSIONS

The microstructure, shear strength, and damage mechanisms of a novel class of Pb-free solders containing RE elements were investigated. Based on the experimental results, the following conclusions can be drawn.

- The addition of La results in the formation of large intermetallic particles ($LaSn_3$) that are dendritic in nature and exist in the eutectic region of the solder microstructure and along the Sn dendrite boundaries.
- The addition of small amounts of La (up to 0.5 wt.%) to Sn-Ag-Cu refines the microstructure by decreasing the length and spacing of the Sn dendrites and decreases the thickness of the Cu_6Sn_5 intermetallic layer at the Cu/solder interface.
- As a result of the change in the microstructure, Sn-Ag-Cu alloys with La additions exhibit a small decrease in ultimate shear strength but significantly higher elongations compared with Sn-Ag-Cu. This has profound implications for improving the mechanical shock resistance of Pb-free solders.
- The $LaSn_3$ intermetallics change the fracture mechanism of the solder joints from a brittle-type fracture (in conventional Sn-Ag-Cu) to ductile fracture, dominated by void nucleation and growth. The increased plastic deformation in the volume of solder leads to higher macroscopic ductility in the La-containing solders.

ACKNOWLEDGEMENTS

The authors gratefully acknowledge the financial support for this research from the Semiconductor Research Corporation (SRC) under Contract No. 2005-KJ-1286 (Dr. H. Hosack, program manager). The authors also thank David Wright, Center for Solid State Science, Arizona State University, for his assistance with evacuating the quartz tubes.

REFERENCES

1. J. Bath, C. Handweker, and E. Bradley, *Circ. Assemb.* 11, 30 (2000).
2. I.E. Anderson, F.C. Foley, B.A. Cook, J. Harringa, R.L. Terpstra, and O. Unal, *J. Electron. Mater.* 30, 1050 (2001).
3. D.H. Kim, P. Elenius, and S. Barrett, *IEEE Trans. Electron. Packaging Manufacturing* 25, 84 (2002).
4. M.E. Loomans and M.E. Fine, *Metall. Mater. Trans. A* 31A, 1155 (2000).
5. A. Schubert, H. Walter, R. Dudek, B. Michel, G. Lefranc, J. Otto, and G. Mitic, *Proc. Int. Symp. on Advanced Packaging Materials Processes, Properties and Interfaces* (Piscataway, NJ: IEEE, 2001), pp. 129–134.
6. D.H. Xiao, J.N. Wang, D.Y. Ding, and H.L. Yang, *J. Alloy Compd.* 352, 84 (2003).
7. J.O. Choi, J.Y. Kim, C.O. Choi, J.K. Kim, and P.K. Rohatgi, *Mater. Sci. Eng. A-Struct.* 383, 323 (2004).
8. G. Pettersen, H. Westengen, R. Hoier, and O. Lohne, *Mater. Sci. Eng. A-Struct.* 207, 115 (1996).
9. J. Chang, I. Moon, and C. Choi, *J. Mater. Sci.* 33, 5015 (1998).
10. A. Ramirez, H. Mavoori, and S. Jin, *Appl. Phys. Lett.* 80, 398 (2002).
11. C.M.K. Wu, C.M.T. Law, D.Q. Yu, and L. Wang, *J. Electron. Mater.* 32, 63 (2003).
12. Z.G. Chen, Y.W. Shi, Z.D. Xia, and Y.F. Yan, *J. Electron. Mater.* 32, 235 (2003).
13. D.Q. Yu, J. Zhao, and L. Wang, *J. Alloy. Compd.* 376, 170 (2004).
14. Z. Xia, Z. Chen, Y. Shi, N. Mu, and N. Sun, *J. Electron. Mater.* 31, 564 (2002).
15. Z.G. Chen, Y.W. Shi, Z.D. Xia, and Y.F. Yan, *J. Electron. Mater.* 31, 1122 (2002).
16. C.M.T. Law, C.M.L. Wu, D.Q. Yu, M. Li, and D.Z. Chi, *IEEE Trans. Advanced Packaging*. 28, 252 (2005).
17. C.M.L. Wu, D.Q. Yu, C.M.T. Law, and L.J. Wang, *Mater. Res*. 17, 3146 (2002).
18. X. Ma, Y. Qian, and F. Yoshida, *J. Rare Earth.* 18, 289 (2000).
19. R.S. Sidhu, X. Deng, and N. Chawla, *Metall. Mater. Trans. A* (2006), in press.
20. X. Deng and N. Chawla, *J. Mater. Sci.* 41, 5731 (2006).
21. A. Ayyar and N. Chawla, *Comp. Sci. Technol.* 66, 1980 (2006).
22. X. Deng, N. Chawla, F. Tang, I.E. Anderson, and B. Glesson, *Proc. Materials Science and Technology 2005* (Warrendale, PA: TMS, 2005), p. 9.
23. X. Deng, G. Piotrowski, N. Chawla, and K.S. Narasimhan, *P/M Sci. Technol. Briefs* 6, 5 (2004).
24. N. Yang, J. Boselli, and I. Sinclair, *J. Microsc.* 201, 189 (2001).
25. X. Deng, R.S. Sidhu, P. Johnson, and N. Chawla, *Metall. Mater. Trans. A*. 36A, 55 (2005).
26. F. Ochoa, X. Deng, and N. Chawla, *J. Electron. Mater.* 33, 1596 (2004).
27. N. Chawla, F. Ochoa, V.V. Ganesh, X. Deng, M. Koopman, K.K. Chawla, and S. Scarritt, *J. Mater. Sci.: Mater. Electron.* 15, 385 (2004).
28. X. Deng, G. Piotrowski, J.J. Williams, and N. Chawla, *J. Electron. Mater.* 32, 1403 (2003).
29. K.W. Moon, W.J. Boettinger, U.R. Kattner, F.S. Biancaniello, and C.A. Handwerker, *J. Electron. Mater.* 29, 1122 (2000).
30. D.R. Frear, *Mechanics of Solder Alloy Interconnects* (New York: Van Nostran, 1994).
31. S. Kang and A.K. Sarkhel, *J. Electron. Mater.* 23, 701 (1994).
32. J. Glazer, *Int. Mater. Rev.* 40, 65 (1995).
33. H. Okamoto, ed., *Desk Handbook: Phase Diagrams for Binary Alloys* (Materials Park, OH: ASM, 2000), pp. 24–28.

34. S. Beer, G. Frommeyer, and E. Schmid, *Proc. Conf. Magnesium Alloys and their Applications* (1992) pp. 317–324.
35. Y.N. Malinochka, L.N. Bagnyuk, and S.A. Zdorovets, *Russ. Metall.* 1, 76 (1989).
36. R. Kesri and S. Hamar-Thibault, *Z. Metallkd.* 80, 502 (1989).
37. K. Ichikawa and S. Ishizuka, *Trans. Jpn. Inst. Met.* 30, 75 (1990).
38. M.A. Dudek and N. Chawla, *Mater. Characterization* (2006), in preparation.
39. W. Kurz and D.J. Fisher, *Fundamentals of Solidification* (Aedermannsdorf, Switzerland: Trans Tech Publications Ltd., 1998), pp. 1–61.
40. M. Huang, X. Su, F. Yin, P. Zhang, Z. Li, and C. Chen, *J. Alloy Compds.* 309, 147 (2000).
41. P.G. Harris and K.S. Chagger, *Solder. Surf. Mt. Technol.* 10, 38 (1998).
42. N. Chawla and R.S. Sidhu, *J. Mater. Sci.- Mater. Elect.* (2006), in press.